PHYSICAL REVIEW A **90**, 022513 (2014)

High-resolution x-ray-emission study of $1s4p$ and $1s3d$ two-electron photoexcitations in Kr

M. Kavčič
Jožef Stefan Institute, Jamova cesta 39, SI-1001 Ljubljana, Slovenia

M. Žitnik
Jožef Stefan Institute, Jamova cesta 39, SI-1001 Ljubljana, Slovenia
and Faculty of Mathematics and Physics, University of Ljubljana, Jadranska ulica 19, Ljubljana, Slovenia

D. Sokaras, T.-C. Weng, R. Alonso-Mori, and D. Nordlund
SLAC National Accelerator Laboratory, Menlo Park, California 94025, USA

J.-Cl. Dousse and J. Hoszowska
Department of Physics, University of Fribourg, CH-1700 Fribourg, Switzerland
(Received 23 June 2014; published 21 August 2014)

High-energy-resolution photoexcited $K N_{2,3}$ x-ray-emission measurements were carried out on krypton with the excitation energy tuned around the $1s4p$ and $1s3d$ double-excitation thresholds. Comprehensive two-dimensional resonant inelastic x-ray-scattering maps were recorded for the range of excitation and emission energies corresponding to both types of double excitations. The double-excitation signal could be clearly resolved from the dominant $1s$ ionization signal. The latter was subtracted from the measured maps, yielding isolated $1s4p$ and $1s3d$ photoexcitation spectra. Both two-electron excitation spectra are well described by a model spectrum built of consecutive bound-bound discrete transitions and shake-up and shake-off channels giving precise energies and intensities of the corresponding contributions. The obtained results are compared with other existing experimental values based on x-ray-absorption measurements and theoretical predictions.

DOI: 10.1103/PhysRevA.90.022513 PACS number(s): 32.30.Rj, 32.70.−n, 32.80.Fb

I. INTRODUCTION

Atomic inner-shell photoionization can be accompanied by an excitation of another electron into a higher empty atomic level (shake-up) or the continuum (shake-off). Since the photon absorption is described by the one-electron operator, these multiple excitations cannot be described within the independent electron picture and are possible only due to electron-electron interactions and therefore directly probe the correlations between electrons. The presence of satellite lines in the photoinduced x-ray-emission [1–3], Auger [4], or photoelectron spectra [5–7] provides evidence for such multielectron photoexcitations. At photon energies high above the excitation threshold the production of satellite lines is explained by the shake model using sudden approximation [1]. At high excitation energies the photoelectron leaves the atom so fast that the remaining electrons adapt to the sudden change of the potential, and consequently, the probability for the shake process becomes energy independent.

In the case of near-threshold excitation the probability for multielectron excitations depends on the photon excitation energy. In order to study in more detail the structure of near-threshold multielectron photoexcitations, photoabsorption spectroscopy with synchrotron radiation is most commonly used. The multielectron contributions in the photoabsorption spectra are manifested as tiny threshold features superposed on the dominant smooth single-ionization contribution. In addition, the structural effects may prevail in the solid-state and molecular spectra. Noble gases, which are easy to manipulate experimentally and are also easier to handle theoretically, are particularly suited for absorption studies of multielectron excitations. Relatively strong multielectron spectral features have been identified in the measured high-resolution K- and L-edge x-ray-absorption spectra of several noble gases [2,8–15].

Recently, a high-resolution resonant inelastic x-ray scattering (RIXS) spectroscopy was successfully applied to study the $1s3p$ and $1s2p$ near-threshold two-electron atomic processes in argon [16,17]. A small energy shift of the satellite emission line allowed us to separate the multielectron signal from the dominant $1s$ single-ionization contribution and follow its near-threshold intensity dependence to reach an isolated two-electron photoexcitation spectrum. This research demonstrated that despite significantly lower cross sections of the RIXS process compared to those of the absorption, an efficient high-resolution x-ray emission spectrometer combined with a powerful third-generation synchrotron beam line can be successfully applied for multielectron photoexcitation studies of gaseous targets.

Multielectron photoexcitations in krypton were studied extensively using x-ray-absorption spectroscopy [11–15]. Schaphorst *et al.* [13] provided absolute photoabsorption cross sections for [$1snp$,nd] excitations. A detailed theoretical analysis of the measured multielectron spectral features was performed. Later, a natural-linewidth deconvolution technique was applied to the experimental spectra, which were recorded with improved resolution and sensitivity by Kodre *et al.* [14] to reach a clear identification of the multielectron spectral features. Despite using extensive theoretical modeling and the most advanced deconvolution analysis the above-mentioned absorption studies still face the inherent problem of the underlying dominant single-electron photoionization component. This becomes particularly severe in the near-threshold region just above the edge where the $1s$ photoionization

cross section is heavily affected by the core relaxation and postcollision interaction effects [18], and a full quantitative model for the near-edge dependence has not yet been given. Consequently, this problem leads to large uncertainties in the separation procedure and the identification of the strongest multielectron spectral features located just above the single-ionization threshold, and also the comparison of theoretical data with experiments is usually based on only the calculations of energy levels. An exception is the work of Schaphorst *et al.* [13], in which a full quantitative theoretical model was used for the comparison with the absolute experimental cross sections. However, in this case large discrepancies between calculations and experiment were found, especially for the $[1s4p]$ excitations starting around 15 eV above the $1s$ threshold. As pointed out by the authors, these discrepancies might be at least partially attributed to uncertainties of the $1s$ single-ionization cross section in the near-threshold region. In order to provide more accurate experimental data free from this effect, a different experimental technique is needed. As demonstrated in our recent work on Ar, RIXS spectroscopy is able to isolate completely the multielectron features from the single-ionization contribution in the near-threshold region [16,17].

In this work we have applied high-resolution RIXS spectroscopy to extract $[1s4p]$ and $[1s3d]$ two-electron photoexcitations in Kr. The $KN_{2,3}$ emission line was measured precisely while tuning the photon excitation energy across the $[1s4p]$ and $[1s3d]$ excitation thresholds. Using the spectrum measured below the double-excitation threshold as a reference, we were able to resolve the double-excitation satellite features from the diagram line and build a full two-dimensional (2D) RIXS map for both $[1s4p]$ and $[1s3d]$ contributions. Finally, the corresponding double-photoexcitation spectra were obtained from the measured RIXS maps by integrating the measured counts over the emission energy for each excitation energy.

II. EXPERIMENT

Measurements were carried out at the 6-2 wiggler beam line of the Stanford Synchrotron Radiation Lightsource (SSRL). The incident photon energy was tuned with a liquid-nitrogen-cooled Si(111) monochromator having a band pass of $\sim$2.2 eV at the energy of the Kr K absorption edge. The incident flux on the target was $\sim 10^{13}$ photons/s. The incident beam focused down to 150×400 μm^2 was impinging on a static gas cell filled with 2 bars of Kr gas and separated from the ambient atmosphere with 75-μm-thick Kapton windows.

The target x-ray emission was recorded by a multiple-crystal Johann-type hard x-ray spectrometer [19]. In our experiment the Si(777) diffraction order from seven spherically bent analyzers placed on intersecting vertical Rowland circles with a 1 m diameter were used. A silicon drift detector with an energy resolution of about 150 eV at 5.9 keV was employed to detect diffracted x rays. Since the spectrometer operates in air, a He bag was introduced between the crystal analyzers and the detector in order to reduce the attenuation and also the diffuse scattering of the x rays. The overall experimental resolution at the Kr K edge was 2.97 ± 0.07 eV, as determined by measurements of the FWHM of the elastic peaks measured in the 14 290–14 350 eV energy range.

Intensities of these elastic peaks were also used to measure the relative efficiency of the spectrometer as a function of the recorded emission energy. Variations of $\pm 1.6\%$ and $\pm 4.2\%$ were found across the emission energy ranges of the $[1s4p]$ and $[1s3d]$ double excitations, respectively. The energy calibration of the spectrometer was performed by setting the spectrometer to the nominal emission energy given by the motors' positions and scanning the monochromator across this energy in order to record the elastic peak. Nine elastic peaks recorded at different positions of the spectrometer within the energy range of the RIXS planes were used to determine the calibration curve. Finally, a $KM_{2,3}$ emission line of Kr was recorded, and reference emission energies of 14 104.96 eV and 14 112.82 eV [20] were used to determine the offset of the monochromator reading. The final uncertainty of this whole calibration procedure was ± 0.10 eV.

In order to record the full RIXS region for $[1s4p]$ excitations we first set the spectrometer to 14 299 eV and then scanned the monochromator from 14 333 to 14 383 eV. First, five steps of 1 eV were made, followed by 40 steps of 0.5 eV across the $[1s4p]$ threshold and then 25 steps of 1 eV to reach the final excitation energy. The full $[1s4p]$ RIXS map was built by repeating such monochromator scans and moving the spectrometer in 0.5-eV steps each time until the final emission energy of 14 329 eV was reached. The recorded intensities were normalized to the incident photon flux measured by the He ionization chamber. The $[1s3d]$ RIXS map was built in a similar way by scanning the monochromator between 14 393 and 14 512 eV (12 steps of 2 eV followed by 75 steps of 1 eV and, finally, 10 steps of 2 eV) for each energy setting of the spectrometer in the 14 321–14 346 eV range (50 steps of 0.5 eV).

III. DATA ANALYSIS

A. $[1s4p]$ excitations

According to the absorption measurements and the calculated energies, the $[1s4p]$ multielectron excitations are expected in the energy range starting at about 10 eV above the K absorption edge. In order to resolve the $[1s4p]$ multielectron excitation signal in the emission channel we need to look at the $KN_{2,3}$ emission spectrum. Figure 1 shows a comparison of two $KN_{2,3}$ emission spectra recorded at photon energies below and above the $[1s4p]$ ionization threshold. The difference of the two spectra normalized to the low-energy tail of the diagram emission line reveals a $KN - N^2$ satellite line on the high-energy tail of the diagram $KN_{2,3}$ emission line recorded above the $[1s4p]$ threshold. The calculations of the $KN - N^2$ emission spectrum performed in the Dirac-Fock self-consistent field scheme [22] confirm the origin of the satellite line.

Having recorded a full RIXS plane, one can readily also take a look at the RIXS intensity at a given fixed emission energy. Figure 2 shows a comparison of the RIXS intensities, one recorded with the emission energy fixed to the top of the KN satellite line and the second one on the other (low-energy) side, symmetric to the center of the $KN_{2,3}$ diagram line. While the first one exhibits a sharp rise in the signal above 14 339 eV due to opening of the $[1s4p]$ excitation channel, the other exhibits a smooth descending slope of the $1s$ single-ionization channel. The technique of recording a secondary fluorescence

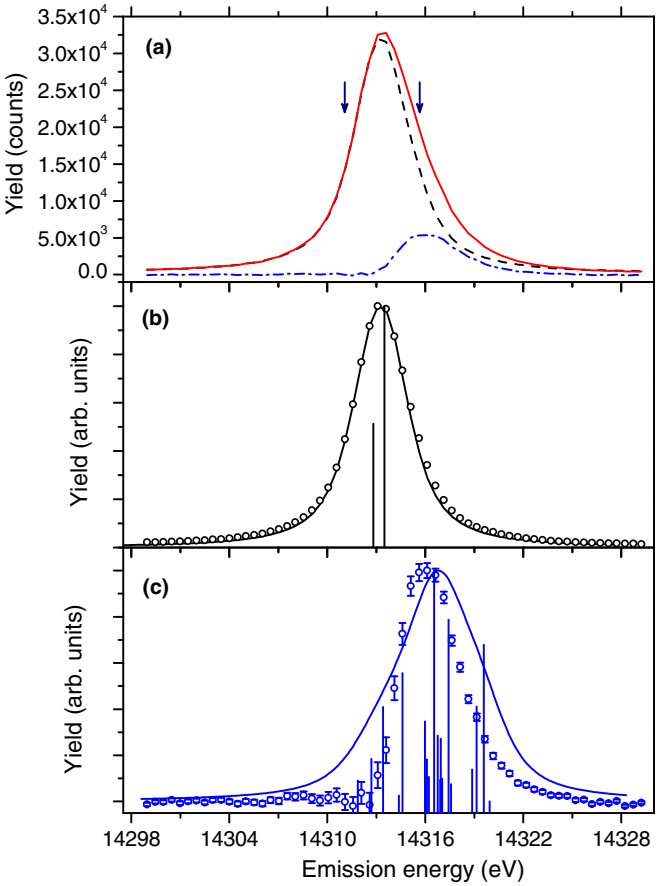

FIG. 1. (Color online) (a) The difference between the Kr $KN_{2,3}$ emission spectra measured at two excitation energies (14 335.76 eV, black dashed line, and 14 382.26 eV, red solid line) below and above the $[1s4p]$ double-excitation threshold reveals a satellite structure on the high-energy tail of the diagram line (blue dash-dotted line). The two arrows indicate emission energies used to obtain the K-N RIXS intensities presented in Fig. 2. (b) The theoretical $KN_{2,3}$ spectrum built from the calculated $[1s]\ ^2S_{1/2}$-$[4p]\ ^2P_{1/2},^2P_{3/2}$ stick spectrum with a natural width of 2.71 eV [21] convoluted with the instrumental response is in perfect agreement with the spectrum measured below the $[1s4p]$ double-excitation threshold. (c) The calculated $[1s4p,4s] - [4p^2,4s4p]$ multiplet structure confirms the origin of the satellite which appears after tuning the excitation energy above the $[1s4p]$ double-excitation threshold.

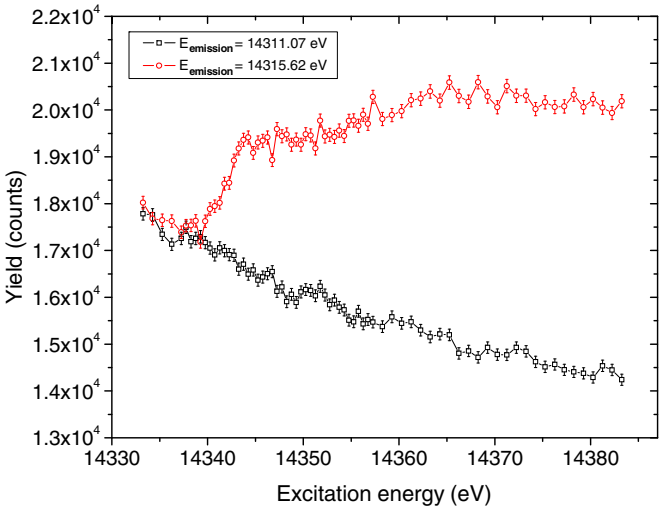

FIG. 2. (Color online) Comparison of the recorded K-N RIXS intensities as a function of the excitation energy with the emission analyzer fixed to 14 315.62 eV, corresponding to the maximum of the $KN - N^2$ satellite line, and to 14 311.07 eV, chosen symmetrically on the other (low-energy) side of the $KN_{2,3}$ diagram line.

with the high-energy-resolution analyzer while tuning the incident photon energy across an absorption edge is referred to as a high-energy-resolution fluorescence detection (HERFD) spectroscopy [23,24] and is usually applied to reduce the core-hole lifetime broadening in absorption spectra. In our case the high-energy resolution in the emission channel is used primarily to resolve the $[1s4p]$ multielectron excitation signal from the dominant $1s$ photoionization signal.

Figures 1 and 2 demonstrate the main advantage of RIXS over the standard absorption spectroscopy: adding an excellent energy resolution of the emission analyzer to the resolution of the beam-line monochromator yields an opportunity to isolate completely the multielectron excitation signal in the vicinity of the main absorption edge. The K-N RIXS signal corresponding to the $1s$ photoionization signal was therefore removed from the recorded spectra following the next procedure. The reference $1s$ single-ionization spectrum was built as an average of the $KN_{2,3}$ emission spectra recorded at the first five excitation energies below the $[1s4p]$ threshold. For each consecutive excitation spectrum the latter was scaled down to compensate for the dropping dependence of the $1s$ ionization cross section and was subtracted from the corresponding emission spectrum to get the pure $KN - N^2$ satellite spectrum. Scaling factors were obtained by matching the low-energy tail (14 299–14 312 eV) of the corresponding spectra with the tail of the reference spectrum (see Fig. 1). Alternatively, the $1s$ photoionization signal was removed by fitting the energy dependence of the RIXS intensity at a fixed emission energy on the low-energy tail of the $KN_{2,3}$ diagram line with an exponential function and subtracting it from the RIXS intensity recorded at the emission energy symmetrically on the other side of the diagram line (see Fig. 2). This was used to check and slightly correct the weighting factors used in first step until consistent intensities were reached by both approaches. The final $KN - N^2$ RIXS map corresponding to $[1s4p]$ double photoionization is presented in Fig. 3.

In Fig. 3 the onset of the $[1s4p]$ excitation is clearly evident at the excitation energy around 14 340 eV. A linear dispersion of the signal characteristic to resonant inelastic scattering [25,26] is observed right at the threshold, which is a signature of discrete $[1s4p]nlnl'$ excitations. Besides a smooth increase of the signal intensity, no significant spectral dependence on the excitation energy is observed farther up, which is characteristic of excitations into continuum.

The fact that we have recorded the emission energy range covering the full $KN_{2,3}$ emission line yields an opportunity to scale our x-ray yields with the absolute photoabsorption cross section reported by Schaphorst *et al.* [13]. Compared to absorption, the $KN_{2,3}$ partial fluorescence yield (PFY) spectrum is slightly modified in the region above the $[1s4p]$ threshold due to a slight decrease of the ω_K fluorescence

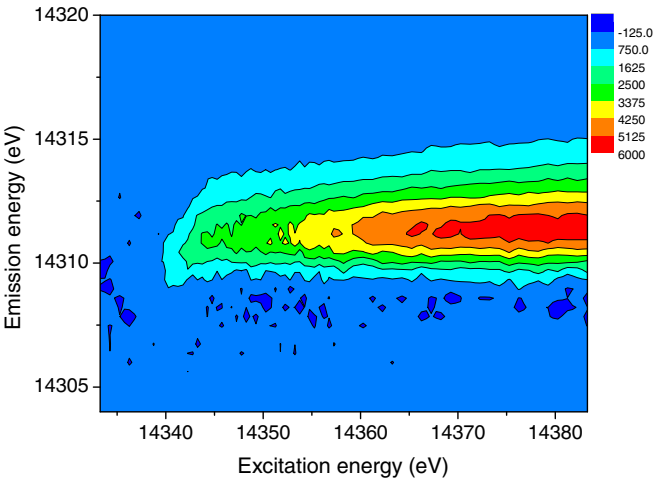

FIG. 3. (Color online) The full $KN - N^2$ RIXS map of Kr. The color scale corresponds to the intensity of the final normalized counts after removing the $1s$ single-photoionization contribution.

yield for the $1s4p$-$4p^2$ transition. This decrease was taken into account by calculating the ratio of oscillator strengths $[1s - 4p]/[1s4p - 4p^2]$ and adding the integrated $KN - N^2$ RIXS intensities multiplied by the factor $([1s - 4p]/[1s4p - 4p^2] - 1)$ to the originally measured $KN_{2,3}$ PFY spectrum. The $[1s - 4p]/[1s4p - 4p^2]$ ratio was calculated as 1.11, but the optimum match to the experimental absorption cross section was reached for the value of 1.045(5). The latter was finally used in the comparison presented in Fig. 4 yielding the scaling factor between integrated RIXS intensities and absolute cross sections.

B. [1*s*3*d*] excitations

In the case of $[1s3d]$ excitations the situation is even more clear. While the KN satellite line of the $KN_{2,3}$ emission line showed up only after comparing the two spectra recorded at

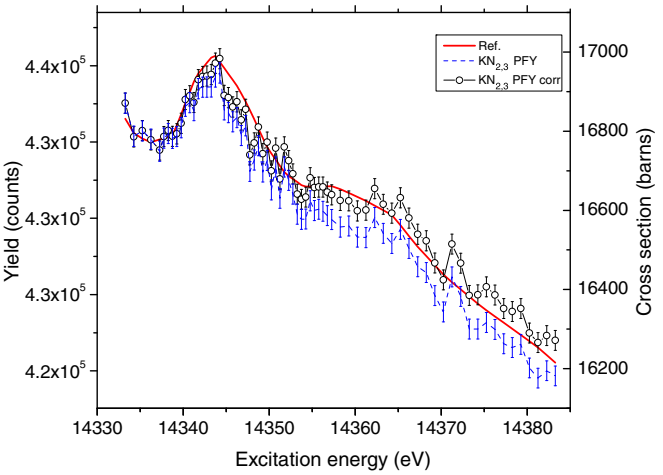

FIG. 4. (Color online) The $KN_{2,3}$ PFY spectrum corrected for the decrease of the fluorescence yield ω_K above the $[1s4p]$ threshold compared with the reference absolute absorption cross section [13]. The comparison serves to provide the scaling factor used to convert the measured x-ray yields into absolute cross sections.

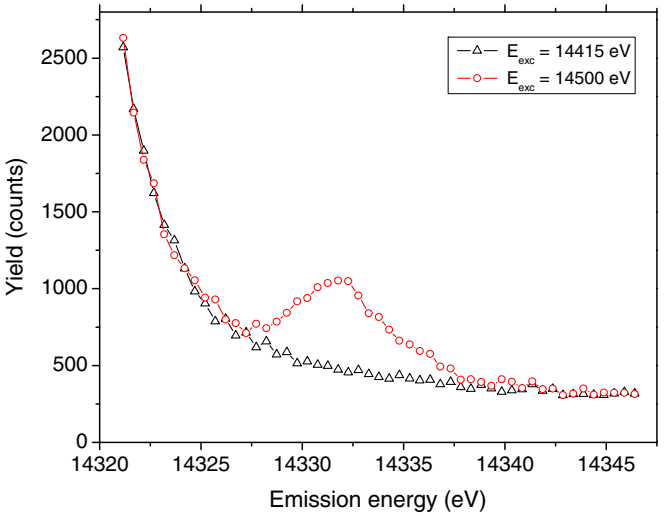

FIG. 5. (Color online) Comparison of the two emission spectra recorded below and above the $[1s3d]$ excitation threshold. A strong KM satellite line superimposed on the tail of the $KN_{2,3}$ diagram line is observed when the excitation energy is tuned above the $[1s3d]$ threshold.

excitation energies below and above the $[1s4p]$ threshold, the KM satellite line is well resolved from the diagram line exhibiting a pronounced structure on the high-energy tail of the $KN_{2,3}$ line, as observed previously in the measurements using an x-ray tube for excitation [27]. This is evident in Fig. 5, which compares two emission spectra recorded at excitation energies below (14 415 eV) and above (14 500 eV) the $[1s3d]$ double-excitation threshold. While in the first case only a smooth tail of the $K\beta_2$ diagram line is present within our range of recorded emission energies, a strong satellite line shows up when the energy is tuned above the $[1s3d]$ threshold.

In order to get the full RIXS map for the case of $[1s3d]$ excitation the $1s$ single-photoionization spectral intensity corresponding to the tail of the diagram line must be subtracted from the measured signal. The average of the first ten spectra recorded at excitation energies below the $[1s3d]$ threshold was used as a reference pure $1s$ spectrum, and the weighting factors were determined by matching the first and last five recorded channels in the corresponding emission spectrum. The final result is shown in Fig. 6. The onset of the $[1s3d]$ excitation is clearly visible around 14 440 eV. A smooth increase indicates a very weak intensity of discrete $[1s3d]nlnl'$ excitations, and the signal is dominated by the excitations into the continuum.

Unfortunately, we cannot use the scaling factor obtained from the $KN_{2,3}$ PFY spectrum in the $[1s4p]$ excitation range for the $[1s3d]$ excitations to get the absolute cross sections. This is because the Kr K absorption edge is situated exactly between the $KN_{2,3}$ diagram line and the $KM - MN$ satellite line. Compared to the diagram line, the intensities of the KM satellite line situated above the K absorption edge are significantly attenuated by the target self-absorption effect. While this self-absorption effect does not influence the measured intensity evolution of the RIXS signal in Fig. 6, it affects its absolute intensity relative to the $KN_{2,3}$ signal.

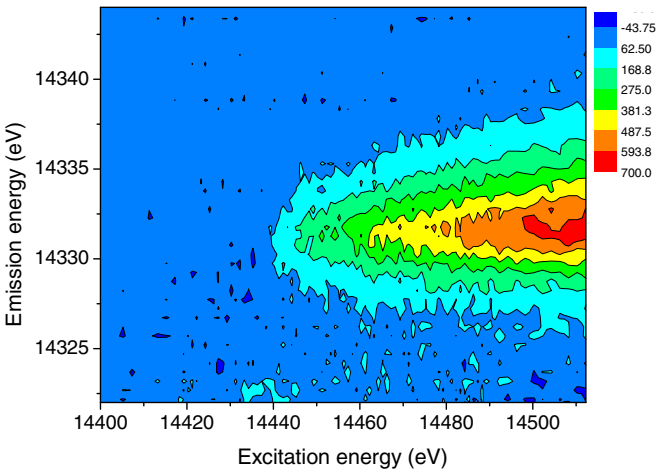

FIG. 6. (Color online) The full $KM - MN$ RIXS map of Kr. The color scale corresponds to the intensity of the final normalized counts after removing the $1s$ single-photoionization contribution.

IV. RESULTS

Since the RIXS cross section depends on both excitation and emission energies (ω_1 and ω_2, respectively), the recorded intensity $I(\omega_1,\omega_2)$ is plotted as a 2D spectral map. In order to reach the excitation spectrum which can be directly compared to absorption measurements, the RIXS signal has to be integrated over the emission energy ω_2 for each excitation energy ω_1. The final $[1s4p]$ excitation spectrum obtained from the $KN - N^2$ RIXS map by projection on the excitation energy axis is presented in Fig. 7. The absolute cross sections were obtained by scaling the $KN_{2,3}$ PFY spectrum to the reference photoabsorption cross section, as already discussed

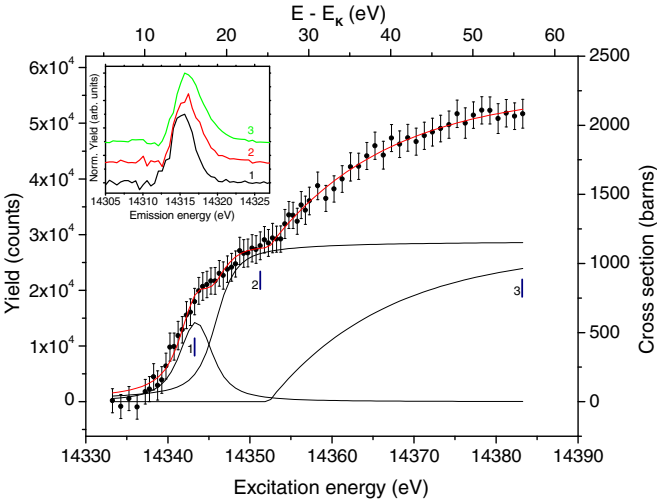

FIG. 7. (Color online) Measured Kr $[1s4p]$ two-electron photoexcitation spectrum fitted with the model [red (gray) solid line] presented in the text. The inset presents the KN satellite emission lines for three separate excitation energies (labeled with bars in the excitation spectrum) corresponding to discrete bound-bound, shake-up, and shake-off transitions (lines 1, 2, and 3, respectively). The individual emission spectra, which are shifted vertically for clarity, exhibit slight energy shifts.

above. Our reported energies of multielectron excitations are given as energy shifts $E - E_K$ from the onset of the one-electron continuum. In this case the zero energy is set to 14 327.17 eV [28].

In order to extract experimental energies and relative intensities the spectrum was modeled using a combination of three types of components describing separate excitation channels. A Lorentzian shape,

$$\sigma_0 \left[\frac{(\Gamma/2)^2}{(E - E_0)^2 + (\Gamma/2)^2} \right], \tag{1}$$

can be used to describe the resonant bound-bound discrete double excitations just at the threshold, with E_0 being the energy of resonant excitation, Γ being the natural lifetime width of the excited state, and σ_0 being the amplitude of the cross section. In order to account for the experimental resolution the resonant discrete channel was actually modeled with a Voigt function corresponding to the convolution of the Lorentzian shape with the Gaussian instrumental response. The width of the latter was fixed to 2.2 eV, corresponding to the resolution of the beam-line monochromator. The lifetime width Γ of the profile was a free-fitting parameter in order to compensate for a slight broadening with respect to the natural linewidth resulting from the multiplet structure of the $[1s4p]nlnl'$ contribution. The shake-up contribution was described by a cumulative Lorentzian distribution,

$$\sigma_0 \left[\frac{1}{2} + \frac{1}{\pi} \arctan\left(\frac{E - E_0}{\Gamma} \right) \right], \tag{2}$$

defined again by the energy position of the shake-up edge, cross-section amplitude, and the lifetime width. Also in this case a convolution with the Gaussian instrumental response was used while the lifetime width Γ was fixed to 2.71 eV [21]. Finally, an exponential saturation profile was used to describe the shake-off contribution when both electrons are ejected into the continuum

$$\sigma_0 \left[1 - \exp\left(-\frac{E - E_0}{\Gamma_S} \right) \right] \{E > E_0\}. \tag{3}$$

In this case E_0 is the threshold of the shake-off channel, σ_0 is the cross-section amplitude, and Γ_S is a parameter defining the saturation range of the shake-off channel. Γ_S is typically much larger than the instrumental response, so the latter was neglected in the fitting model.

The overall profile of the excitation spectrum is well reproduced by the model spectrum presented above. Experimental energies and cross sections for separate excitation channels extracted from the fit are tabulated in Table I, where they are compared to other existing theoretical values. In absorption experiments, usually, no specific experimental energies are reported especially for the multielectron excitations closest to the single-ionization threshold, and only calculated energy markers are used to identify the spectral features. On the other hand, the RIXS approach provides an isolated spectrum which also yields the experimental values obtained by relatively simple modeling of the measured spectrum. As we can see from Table I, the extracted experimental energies are very close to the calculated Hartree-Fock (HF) average multiplet values. For the discrete bound-bound resonance, in addition to the $[1s4p]5p^2$ state, the $[1s4p]4d^2$ state is also accessible

TABLE I. Energies and cross sections of separate $[1s4p]$ excitation channels extracted from the fit. The σ_0/σ_{1s} ratios obtained in the present work were derived using the theoretical $1s$ ionization cross section quoted in [13].

	$E - E_K$ (eV)	
Excitation	This work	Theory
$[1s4p]5p^2$	16.3(3)	16.06 [12], 15.9 [14]
$[1s4p]4d^2$		16.60 [12], 16.5 [14]
$[1s4p]5p$	18.7(4)	19.32 [12], 19.2 [14]
$[1s4p]$	25.1(4)	26.67 [12], 26.6 [14]
	σ_0 (barns),	σ_0/σ_{1s} (%)
Excitation	this work	This work Theory
$[1s4p]5p$	1165(95)	9.6(8) 12.3 [13]
$[1s4p]np$		5.1 [13]
$[1s4p]$	1095(105)	9.0(9) 6.9 [13]

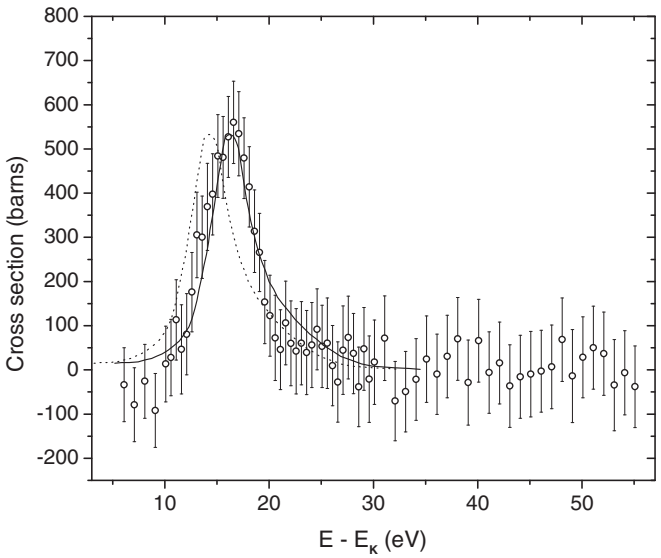

FIG. 8. Experimental Kr $[1s4p]nln'l'$ resonant double-photoexcitation spectrum compared with the theoretical double bound-bound-transition cross section [13]. The original theoretical spectrum (dotted line) shifted by 2 eV (solid line) is in excellent agreement with the experiment.

by the $1s$-$4p$ transition from the admixture of the $[4p^2]4d^2$ configuration in the ground state, but this could not be resolved in our experiment. In addition to energies, cross sections corresponding to the different excitation channels were extracted from the fit.

The only example in the literature where a full quantitative theoretical model for Kr $[1s4p]$ multielectron excitations was built is the work by Schaphorst *et al.* [13], which is based on the single-configuration HF scheme in which, however, the initial- and final-state configuration interaction (CI) was neglected. In [13] the double-excitation shake-up and shake-off cross sections are given relative to the $1s$ ionization cross section. For the latter a value of 12 104 barns was obtained from the calculations for an incident photon energy of 14 800 eV. Our cross sections given in Table I are therefore also given relative to this theoretical value. While in the absorption study by Schaphorst *et al.* [13] the theoretical shake-up cross section near threshold rises far above the measurements (the discrepancy amounts to a factor of ∼4), our corresponding cross section significantly exceeds their experimental values and thus significantly reduces this previous discrepancy with the theory. This is attributed to the accurate separation of the multielectron signal, which avoids large uncertainties in the $1s$ single-ionization cross section. However, the theoretical $[1s4p]$ shake-up cross section near threshold still overestimates our experimental cross section by almost a factor of 2.

It is also very interesting to compare only the resonant part of both excitation spectra. Of course the intrinsic natural spectral shape is broadened by the experimental energy resolution. In absorption measurements by Schaphorst *et al.* [13] a Si(220) monochromator was used, yielding ∼0.5 eV higher experimental resolution compared to ours. However, the shape is dominated by the lifetime width Γ, which is significantly broader compared to the resolution [the Γ value obtained in our fit was 3.8(6) eV], so that the influence of the slightly different experimental resolution is almost negligible. We have therefore subtracted from the excitation spectrum of Fig. 7 the smooth shake-up and shake-off model components, and the resulting clean $[1s4p]nln'l'$ spectrum is compared to the theoretical one in Fig. 8. As shown, if the theoretical resonant spectrum of Schaphorst *et al.* is shifted by 2 eV, excellent agreement with our experimental data is observed. This might at first suggest that the initial- and final-state CI, which was not considered in the calculations, does not play a very significant role. However, it is necessary to note that our experimental excitation spectrum is actually proportional to the differential RIXS cross section taken along the particular emission angle close to the incident polarization axis defined by the Bragg angle of the spectrometer. While x-ray emission from an ionized atom is practically isotropic, this, in principle, does not hold for the fluorescence angular pattern emitted by excited atomic states with well-defined total angular momentum [29]. As already pointed out in our work on Ar [16], while there is no ambiguity in the measured shape, the absolute cross section might be slightly suppressed due to the fact that in the direction of the incident polarization the resonant $J = 1 \rightarrow J = 0$ fluorescence contribution is absent.

The $[1s3d]$ excitation spectrum was deduced similarly from the measured $KM - MN$ RIXS map by projecting the total RIXS signal on the excitation energy axis. As already explained in Sec. III, the scaling procedure used to obtain the absolute cross sections for the $[1s4p]$ excitations is not applicable to the $[1s3d]$ excitation spectrum due to the target self-absorption. We have therefore normalized our $[1s3d]$ excitation spectrum to the absolute experimental and theoretical absorption $[1s3d]$ cross sections from [13] at high excitation energies (above 14 490 eV) where the spectra are merging. The final $[1s3d]$ excitation spectrum is presented in Fig. 9. The spectrum was again modeled by summing up the contributions of the resonant discrete excitations and the shake-up and shake-off processes. The fitted model spectrum reproduces well the measured excitation spectrum.

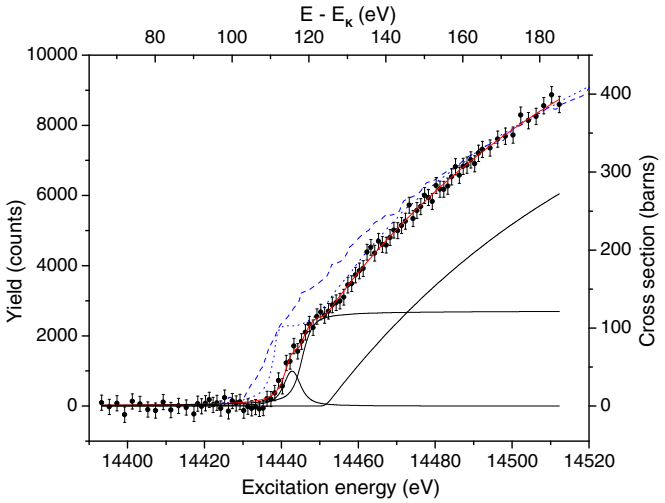

FIG. 9. (Color online) Experimental Kr $[1s3d]$ double photoexcitation spectrum fitted with the model (red solid line) presented in the text. The spectrum is normalized to the high excitation energy part of the absolute experimental (dashed line) and theoretical (dotted line) absorption $[1s3d]$ cross sections from [13].

The corresponding energies and relative intensities extracted from the fit are given in Table II.

The final energies of the resonant, shake-up, and shake-off terms extracted from the fit are in good agreement with the theoretical Dirac-Fock multiplet center energies and experimental values, both given by Kodre *et al.* [14]. In that work the experimental values were obtained by fitting a model combination of separate excitations channels to the reduced absorption cross section, which was obtained using an exponential ansatz to describe the continuum contribution within the measured *1s* total absorption cross section. Our excitation spectrum provides only intensities of separate excitation channels normalized relative to each other. In order to compare with other existing absorption values which are given relative to the $1s$ ionization cross section we have used the absolute scale presented in the right axis of Fig. 9 and $1s$ single-ionization cross section calculated by Schaphorst *et al.* [13] for an incident photon energy of 14 800 eV. Our shake-up model component levels up at 1% relative to this reference $1s$ ionization cross-section value. This is slightly smaller than other absorption values yielding 1.3%–1.4%. The shake-off value obtained from our fit reaches 4.1%, in agreement with the value reported by Schaphorst *et al.,* who built the model spectrum from *ab initio* calculated cross sections that reached good agreement with the experimental absorption spectrum. Also the ratio of our shake-off to shake-up cross sections is close to the theoretically predicted value of 3.1 [13], which is approached in the sudden approximation regime. On the other hand, Kodre *et al.* [14] used a reduced absorption spectrum and fitted it with a model built from the resonant, shake-up, and shake-off excitation components. Compared to that of Schaphorst *et al.,* their fit yielded a 6 times smaller value for the shake-off component (0.6%). Such a large discrepancy between the two reported shake-off values can be attributed precisely to the main problem characterizing absorption studies, namely, the proper choice of the $1s$ continuum baseline onto which the multielectron contribution is superimposed.

TABLE II. Same as in Table I, but for the $[1s3d]$ excitation channels.

	$E - E_K$ (eV)		
Excitation	This work	Other works	Theory
$[1s3d]4d5p$	115.6(4)	114 [14]	113 [14]
		118 [14]	116 [14]
$[1s3d]4d$	118.2(4)	119 [14]	118 [14]
$[1s3d]$	124.4(7)	126 [14]	124 [14]
	σ_0 (barns),	σ_0/σ_{1s} (%)	
Excitation	this work	This work	Other works
$[1s3d]4d$	122(11)	1.01(9)	1.3 [14]
			1.4 [13]
			1.4 [30]
$[1s3d]$	495(40)	4.1(3)	3.7 [13], 0.6 [14]

V. CONCLUSIONS

A high-energy-resolution crystal x-ray-emission spectrometer was used to record the Kr $KN - N^2$ and $KM - MN$ RIXS maps near the $[1s4p]$ and $[1s3d]$ excitation thresholds. A clean separation of the double-excitation signal from the $1s$ continuum contribution was obtained, yielding isolated $[1s4p]$ and $[1s3d]$ two-electron excitation spectra. The extracted spectra are described by a simple model built of consecutive bound-bound, shake-up, and shake-off contributions giving precise energies and intensities of separate spectral features. The energies are in good agreement with the calculated values for both excitation spectra. For the $[1s4p]$ excitations the resonant bound-bound excitation component matches well the calculated double-excitation spectrum. The intensity of the shake-up component is still overestimated by the theory, but compared to those for the absorption data, these discrepancies are diminished. In the case of $[1s3d]$ excitation the relative intensity of the shake-up component is slightly lower compared to the theoretical prediction and the analysis of former experimental absorption data, while the shake-off to shake-up intensity ratio is close to the theoretically predicted value. This work demonstrates the potential of RIXS spectroscopy to provide clean multielectron excitation spectra and remove possible ambiguities in the absorption spectra caused by the uncertainties of the dominant single-ionization cross section in the near-threshold region.

ACKNOWLEDGMENTS

This work is supported by the Slovenian Ministry of Education, Science and Technology through research program P1-0112. J.C.D. and J.H. also acknowledge the financial support of the Swiss National Science Foundation. The Stanford Synchrotron Radiation Lightsource is a National User Facility operated by Stanford University on behalf of the US Department of Energy, Office of Basic Energy Sciences.

[1] T. Åberg, Phys. Rev. **156**, 35 (1967).
[2] R. D. Deslattes, R. E. LaVilla, P. L. Cowan, and A. Henins, Phys. Rev. A **27**, 923 (1983).
[3] P.-A. Raboud, M. Berset, J.-Cl. Dousse, Y.-P. Maillard, O. Mauron, J. Hoszowska, M. Polasik, and J. Rzadkiewicz, Phys. Rev. A **65**, 062503 (2002).
[4] G. B. Armen, T. Åberg, K. R. Karim, J. C. Levin, B. Crasemann, G. S. Brown, M. H. Chen, and G. E. Ice, Phys. Rev. Lett. **54**, 182 (1985).
[5] M. O. Krause, T. A. Carlson, and R. D. Dismukes, Phys. Rev. **170**, 37 (1968).
[6] P. H. Kobrin, S. Southworth, C. M. Truesdale, D. W. Lindle, U. Becker, and D. A. Shirley, Phys. Rev. A **29**, 194 (1984).
[7] F. Heiser, S. B. Whitfield, J. Viefhaus, U. Becker, P. A. Heimann, and D. A. Shirley, J. Phys. B: At. Mol. Opt. Phys. **27**, 19 (1994).
[8] J. M. Esteva, B. Gauthe, P. Dhez, and R. C. Karnatak, J. Phys. B: At. Mol. Opt. Phys. **16**, L23 (1983).
[9] K. G. Dyall and R. E. LaVilla, Phys. Rev. A **34**, 5123 (1986).
[10] M. Deutsch, N. Maskil, and W. Drube, Phys. Rev. A **46**, 3963 (1992).
[11] M. Deutsch and M. Hart, Phys. Rev. A **34**, 5168 (1986).
[12] M. Deutsch and M. Hart, Phys. Rev. Lett. **57**, 1566 (1986).
[13] S. J. Schaphorst, A. F. Kodre, J. Ruscheinski, B. Crasemann, T. Åberg, J. Tulkki, M. H. Chen, Y. Azuma, and G. S. Brown, Phys. Rev. A **47**, 1953 (1993).
[14] A. Kodre, I. Arčon, J. Padežnik Gomilšek, R. Prešeren, and R. Frahm, J. Phys. B: At. Mol. Opt. Phys. **35**, 3497 (2002).
[15] M. Deutsch and P. Kizler, Phys. Rev. A **45**, 2112 (1992).
[16] M. Kavčič, M. Žitnik, K. Bučar, A. Mihelič, M. Štuhec, J. Szlachetko, W. Cao, R. Alonso Mori, and P. Glatzel, Phys. Rev. Lett. **102**, 143001 (2009).
[17] M. Žitnik, M. Kavčič, K. Bučar, A. Mihelič, and R. Bohinc, J. Phys. Conf. Ser. **488**, 012014 (2014).
[18] J. Tulkki and T. Åberg, J. Phys. B: At. Mol. Phys. **18**, L489 (1985).
[19] D. Sokaras, T.-C. Weng, D. Nordlund, R. Alonso Mori, P. Velikov, D. Wenger, A. Garachtchenko, M. George, V. Borzenets, B. Johnson, T. Rabedeau, and U. Bergmann, Rev. Sci. Instrum. **84**, 053102 (2013).
[20] R. Deslattes, E. G. Kessler, Jr., P. Indelicato, L. de Billy, E. Lindroth, and J. Anton, Rev. Mod. Phys. **75**, 35 (2003).
[21] J. L. Campbell and T. Papp, At. Data Nucl. Data Tables **77**, 1 (2001).
[22] K. G. Dyall, I. P. Grant, C. T. Johnson, F. A. Parpia, and E. P. Plummer, Comput. Phys. Commun. **55**, 425 (1989).
[23] K. Hämäläinen, D. P. Siddons, J. B. Hastings, and L. E. Berman, Phys. Rev. Lett. **67**, 2850 (1991).
[24] F. M. F. de Groot, M. H. Krisch, and J. Vogel, Phys. Rev. B **66**, 195112 (2002).
[25] A. Kotani and S. Shin, Rev. Mod. Phys. **73**, 203 (2001).
[26] F. Gel'mukhanov and H. Ågren, Phys. Rep. **312**, 87 (1999).
[27] J.-Cl. Dousse and J. Hoszowska, Phys. Rev. A **56**, 4517 (1997).
[28] M. Breinig, M. H. Chen, G. E. Ice, F. Parente, B. Crasemann, and G. S. Brown, Phys. Rev. A **22**, 520 (1980).
[29] S. H. Southworth, D. W. Lindle, R. Mayer, and P. L. Cowan, Phys. Rev. Lett. **67**, 1098 (1991).
[30] J. Padežnik Gomilšek, A. Kodre, I. Arčon, A. M. Loireau-Lozac'h, and S. Bénazeth, Phys. Rev. A **59**, 3078 (1999).